

AN OVERVIEW OF RECENT EXPERIMENTAL STUDIES CONDUCTED IN ONERA S3CH TRANSONIC WIND TUNNEL

R. Bur*, V. Brion*, P. Molton*

***ONERA, The French Aerospace Lab, Meudon, France**

Keywords: *wind tunnel, transonic flow, shock wave, boundary layer, flow control*

Abstract

This paper has the objective to present an overview of recent experimental studies conducted in the S3Ch transonic wind tunnel of the ONERA Meudon centre. Experimental investigations have been carried out on a civil transport aircraft power plant configuration to point out the complex wing / pylon / nacelle interference. Control of turbulent buffet phenomenon was performed on a swept wing by means of mechanical and fluidic vortex generators actuators. As a follow up study, the problem of laminar flow over wings in transonic flow conditions was tackled by an in-depth analysis of the shock dynamics in laminar conditions.

1 Introduction

A large scope of experimental studies dealing both with external and internal aerodynamics have been performed since several decades in the S3Ch transonic wind tunnel of the ONERA Meudon centre. Some examples of studies achieved in this facility are then listed: wing / nacelle interference, buffet over airfoil, air intake efficiency of military aircrafts, afterbody drag evaluation and missile jet signature, base buffeting of launcher afterbodies.

Recently, the capability of the wind tunnel was increased by improving the optical access around its test section. So, even if flow diagnostic always needs classical probe-like measurements, the optical non-intrusive measurement techniques allow producing more in-depth analysis of complex flow field configurations.

After a description of the facility, results are presented on recent experimental studies where optical measurements are strongly involved to finely analyze complex flow field topologies. The first study is devoted to a civil transport aircraft power plant configuration in order to clearly understand the flow behaviour in the wing / pylon / nacelle interference region. The second study deals with a better understanding of the turbulent buffet phenomenon on a swept wing so as to optimize its control by using mechanical and fluidic vortex generators actuators. At last, due to a growing interest of laminar flows in an overall context of drag reduction for commercial aircrafts, studies on laminar flow configurations are presented, and more precisely results of the shock dynamics on a wing profile without tripping the boundary layer at its leading edge.

2 Wind Tunnel Description and Means of Investigation

The S3Ch wind tunnel [1] is a transonic facility involving flow velocities from Mach 0.3 to 1.2 with an optimal turbulence rate of 0.15% (see Fig. 1). It is a continuous closed-circuit wind tunnel operated at atmospheric stagnation pressure, featuring stagnation temperature of approximately 310K (possibly less, 290K, thanks to a thermal exchanger device). The facility is powered by a 3.5MW two-stage motor-ventilator group, equipped with 24 blades, which rotates at a fixed rotational speed of 1500rpm. The test section has a 0.76m × 0.8m rectangular shape and is 2.2m in length.

The wind tunnel test section uses lower and upper solid walls, but also deformable walls

whose shapes are adapted for each flow condition based on a steady flow hypothesis so as to reproduce far-field (infinite) conditions. This eliminates the need for data correction required in straight wall tunnel tests. Side walls are equipped with schlieren quality windows. The flow velocity is adjusted by a downstream sonic throat, which warrants a $\pm 10^{-4}$ uncertainty of the Mach number value.



Fig. 1. View of the S3Ch wind tunnel of the ONERA Meudon centre

The facility is equipped with an axial model string composed of an internal balance system allowing incidence and yaw angle variations up to 60° . Compressed air supply is available: for instance, the system can supply 2kg/s mass flow rate at 40bar and 300K or 0.6kg/s at 60bar and 1000K. Flow extraction by a vacuum pump (0.1kg/s) or by an ejector system (up to 4kg/s) can be provided if necessary. The model can be mounted through the sidewalls and equipped with an internal or external balance. Data is acquired and processed by a 48 channels system and allows the connection of additional sensing systems.

Flow analysis is performed thanks to classical (pressure taps, probes, Kulite sensors) and optical (PSP and TSP, pressure and temperature sensitive paints; PIV, particle image velocimetry; LDV, laser Doppler velocimetry) measurement techniques.

3 Experimental Investigation of an Aircraft Powerplant Configuration

3.1 Context

The diameter of the turbofan engines for civil transport aircraft has increased in the last decades to improve the propulsion efficiency and reduce the fuel consumption. Even for long range aircraft, for which two big engines or four smaller engines are proposed, the two engine versions are often selected for global economic reasons. This tendency, coupled with the different constraints at aircraft level (ground clearance, short pylon preferable for heavy engines for structural reasons), leads to relative engine positions closer to the wing. For the next generation of aircraft projects, the intensity of the interactions between the engine and the airframe could be important and generate critical phenomena. In addition, when the engine is installed closer and closer to the airframe, the evolutions of the interactions are no more linear and it is difficult to extrapolate the actual conventional solutions in term of engine installation.

So, Airbus France and ONERA have decided to launch the research projects “JEDI” (JEt Development Investigations) and “EFAPS2” (Environmentally Friendly Aircraft and Propulsion System 2).

3.2 Test Set-up and Model

The configuration investigated is a wall-to-wall swept wing equipped with a pylon, an engine and an air supply stick (Fig. 2).

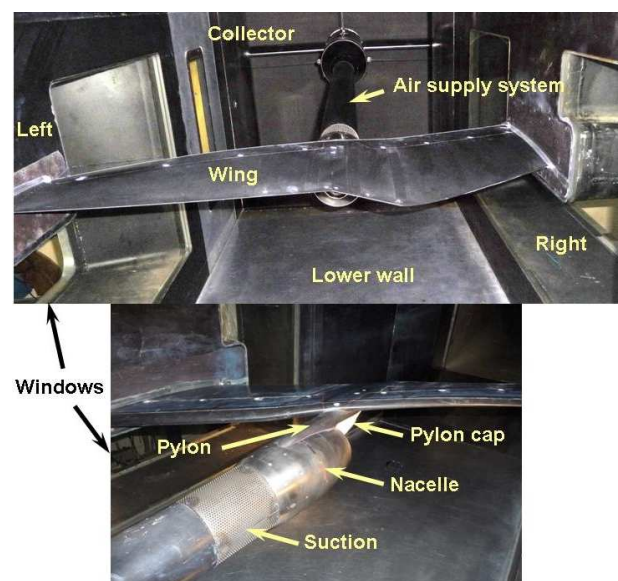


Fig. 2. View of the model and the air supply system upstream of the nacelle

The engine installation is slightly different from the one of a present aircraft: the nacelle has a relative much bigger size and is much closer to the wing, with a specific pylon shape. Such configuration represents what could be the engine installation of future aircraft. The nacelle was studied and manufactured to be able to simulate the engine fan and core jets, in term of pressure ratio, but also to simulate the higher temperature of the core jet by using a heater. An air supply system was installed upstream of the nacelle and delivered pressurized air for the jets. A boundary layer suction system was adapted too in order to diminish the incoming boundary layer from the air supply stick.

The main geometrical characteristics of the model are: a wing span of 0.8m, a reference aerodynamic chord of 0.44m and a nacelle diameter D of 0.1m at the trailing edge. Specific adapted upper and lower walls have been installed. These walls have three-dimensional shapes and have been designed to reduce the wall corrections for this kind of model.

3.3 Main Results

Many different measurement techniques were applied to obtain an accurate description of the jets development with respect to the pressure ratios of the engine jets and the free-stream transonic (cruise and descent phase) Mach number values M_0 under study [2]. Static pressure measurements are obtained on the wing, the pylon and the nacelle and measurements of the characteristics of the fan and core jets (mass flows, total pressures and temperatures) are performed with rakes located inside the nozzle.

Emphasis has been put to accurately quantify the thermal impact of the jets on the pylon. So, TSP measurements have been performed by means of an endoscope mounted on the test section lower wall (see Fig. 3).

Windows are installed on side walls to allow PIV and LDV measurements to be carried out. The PIV plan is coming downstream of the model thanks to a beam installed into the test section. Flow visualizations by tomoscopy (as in Fig. 4) allow verifying the quality of the flow and selecting the flow regions to analyze.

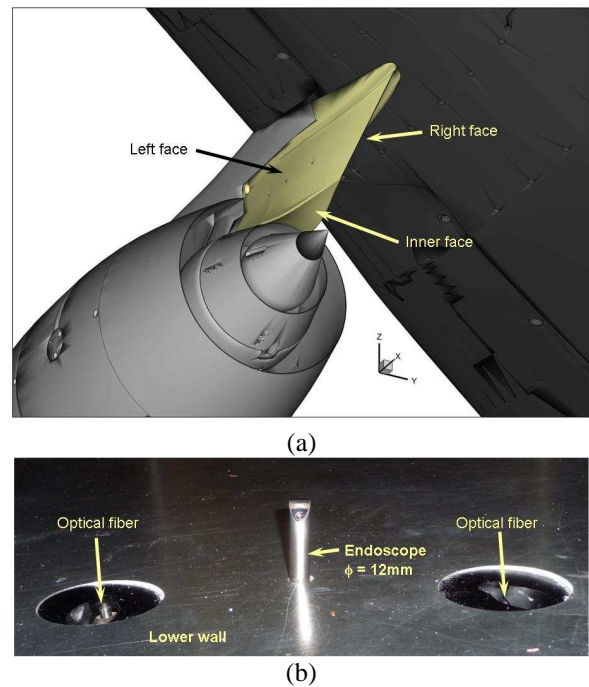


Fig. 3. Sketch of the pylon (a) and view of the endoscope mounted on the test section lower wall

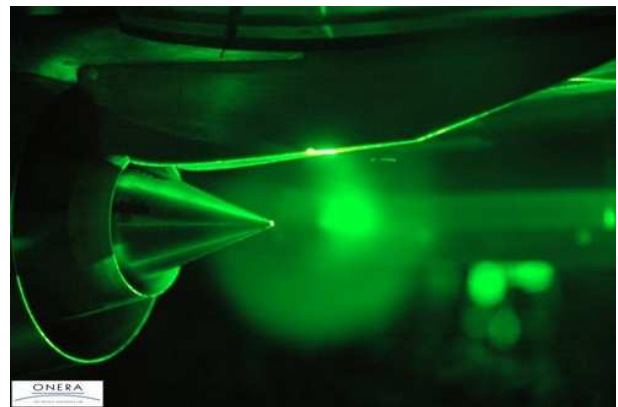


Fig. 4. Flow visualization by tomoscopy in the near wake of the nacelle

Figure 5 summarized measurement results obtained on such complex configuration at cruise condition ($M_0 = 0.8$). TSP measurements have allowed quantifying the thermal impact of the high subsonic cold fan jet and the supersonic hot core one on the pylon structure. Moreover, the mixing of jets is pointed out thanks to three-component LDV measurements in the near wake (one and two diameter D planes downstream) of the nacelle, by plotting the iso-values of the fluctuating axial velocity component. At the plane $X/D = 1$, the level of these fluctuations is evidenced in the mixing layers (external flow - fan jet, fan jet - core jet), into the plug wake and the wake of the rear part

of the pylon. At $X/D = 2$, even if the fluctuations level remains almost the same in the mixing layer between the external flow and the fan jet, the mixing of engine jets is effective and leads to a decrease of the fluctuations intensity inside the hot core jet.

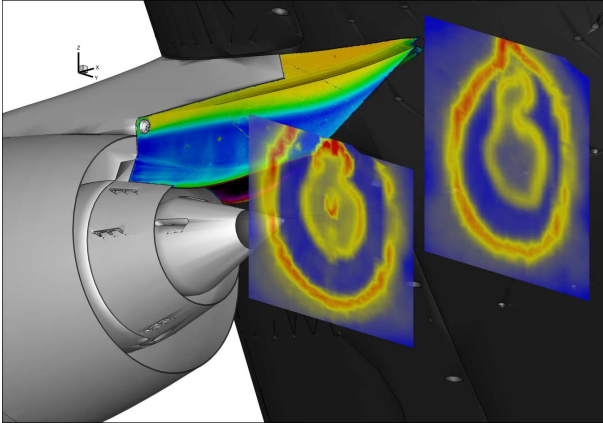


Fig. 5. TSP measurements on the pylon and LDV measurements in the near wake of the nacelle ($M_0 = 0.8$)

4 Control of Turbulent Buffet Phenomenon on a Swept Wing

4.1 Context

The shock wave/boundary-layer interaction on the upper side of a wing at a high Mach number and/or high angle of attack induces a massive flow separation, which can lead to an instability. This phenomenon is a global flow instability known as “buffet” and can further lead to structural vibrations (“buffeting”). Buffet results in lift and drag variations that greatly affect the aircraft aerodynamics and, as such, it limits aircrafts’ flight envelope, because a margin of 30% with the lift coefficient of cruise conditions has to be respected by design standards.

A previous experimental study on a two-dimensional OAT15A profile [3,4] allowed a precise description of the aerodynamic conditions for buffet onset and a characterization of the periodic motion of the shock wave classically observed in two-dimensional buffet.

Then, ONERA has launched an internal research project named “PRF BUFET”N Co” [5] (Projet de Recherche Fédérateur BoUcle FÉrmée appliquée au Tremblement 3D :

démonstration du Contrôle). The main goal of the present study is the open and closed-loop control of buffet on a half-model with a swept wing. Because the separation of the boundary layer is at the origin of buffet, the objective of this experimental study is to postpone this buffet onset by suppressing or decreasing the separation zone by using control devices.

4.2 Test Set-up and Model with Control Devices

The experimental arrangement is shown in Fig. 6. The model is composed of a swept wing attached on a half-fuselage and was designed mostly like the supercritical OAT15A airfoil. The swept angle at the leading edge is equal to 30° . The wing twist was adapted to ensure a constant pressure along the span in cruise conditions, as well as a shock parallel to the leading edge. From root to tip, the chord varies between 240 and 200mm over a span of 704mm. In the end, no separation at the wing root was ensured thanks to adapted profiles and twist in that region.



Fig. 6. View of the experimental set-up

The free-stream Mach number M_0 is set at 0.82 for all tested configurations. The angle of attack α of the model can be varied between 2° and 4° by a mechanical system and/or a proper adjustment of the adaptive walls. By continuously varying α one could accurately find the value for buffet onset. The Reynolds number based on the mean aerodynamic chord, i.e., 220mm, is equal to 2.5×10^6 . Boundary layer transition is triggered on the model by using a carborundum strip located at 7% of the chord on both the upper and lower sides of the model, as well as on the fuselage. The model is equipped with 49 static pressure taps, 39

unsteady Kulite pressure transducers, and 6 accelerometers.

Four control devices are investigated and four dedicated covers have been manufactured. The first control device is of passive control type, i.e., mechanical vortex generators (VGs). Because of the swept wing, only co-rotating VGs are considered here, with a triangular shape. The other three control devices are active: two continuous fluidic VGs and one pulsed fluidic VG. The fluidic VGs consist in small nozzles with a supersonic exit flow, the exit diameter of the nozzles being equal to 1mm. The pitch angle defined between the jet direction and the local wall tangent, is equal to 30° . The orientation of the jets with respect to the leading edge of the model is an important parameter; this is the reason why it has been studied numerically [6], in order to define the most interesting skew angles to be tested. Thus, two skew angles (30 and 60°) for continuous fluidic VGs have been tested and one (60°) for the pulsed fluidic VGs. These pulsed fluidic VGs consist in ONERA homemade piezoelectric actuators supplied with compressed air and driven by an electric square signal. More information on the characteristics of each VGs' configuration is given in [7].

4.3 Main Results

The first part of the study consists in searching for buffet onset conditions by varying the incidence of the model and then in qualifying the reference flow in the presence of buffet. During this first stage, pressure measurements around the model were performed (steady and unsteady pressure), as well as visualizations of the flow by viscous coating. In the second part of the study, the effectiveness of various control types was evaluated using the same measurements. Then, the flow fields for the baseline and for some controlled configurations were measured using two-components PIV and three-components LDV systems [7].

Figure 7 shows a comparison of oil flow visualizations between the clean configuration and the controlled ones with mechanical and fluidic VGs, when the buffet regime is well established at the incidence α equal to 3.5° .

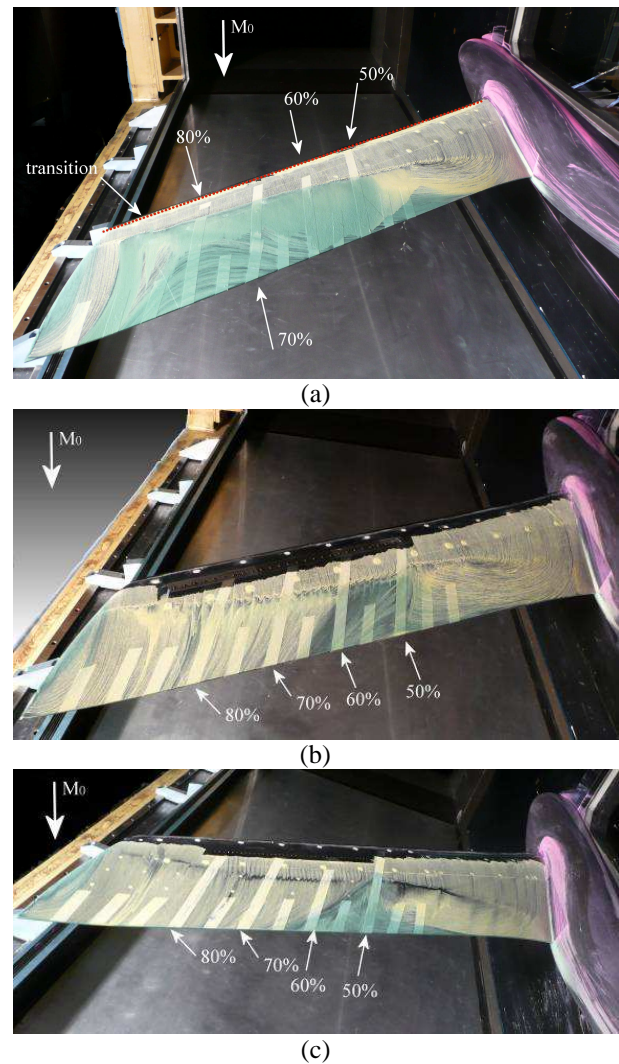


Fig. 7. Oil flow visualizations for the clean configuration (a) and the controlled ones with mechanical (b) and fluidic (c) VGs ($\alpha = 3.5^\circ$ and $M_0 = 0.82$)

For the clean configuration, the flow is fully separated downstream of the shock foot. However, the backflow cannot cross the shock foot due to the pressure jump. The massive separated flow extends from the foot shock up to the trailing edge of the wing. One can remark that the flow is fully attached at the wing root, and no corner separation is observed.

When control by mechanical VGs is applied, flow separation has been suppressed over most of the wing span except between $Y/b = 0.5$ and 0.6 , where a recirculation zone remains. Just downstream of the VGs, one can observe an interesting three-dimensional flow pattern in the shock foot region and the footprint of the longitudinal vortices created by the VGs. These vortices deform the shock along the span

leading to a very complex but almost periodic three-dimensional shock/vortices interaction. The flow topology is very similar when control by fluidic VGs is applied: the separation is almost suppressed and a limited separated zone close to the wing root remains, which is similar to the mechanical VGs' case.

Figure 8 shows a comparison of the C_p distributions at $Y/b = 0.7$ between the baseline, mechanical and fluidic VGs configurations. This span-wise section is representative of the most separated region on the upper wing. The results show that the control effect on the pressure plateau level upstream of the shock is negligible. The mean shock location has been shifted more downstream on the wing at around $X/c = 0.55$ because of the separation alleviation for all controlled cases. The shock seems to be located more downstream in the fluidic VGs' case than for the mechanical VGs.

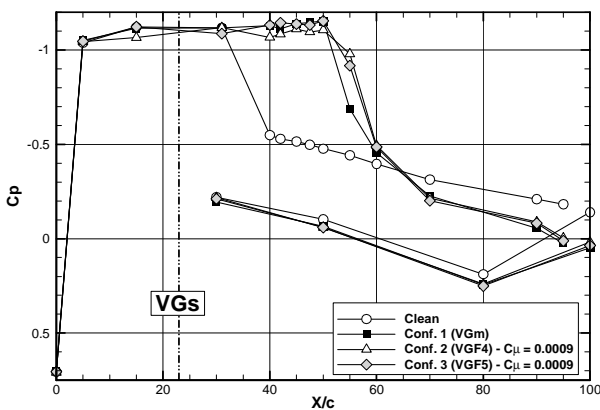


Fig. 8. Comparison of C_p distributions between the clean configuration and the controlled ones with mechanical and fluidic VGs ($\alpha = 3.5^\circ$ and $M_0 = 0.82$)

The root mean square (rms) pressure chord-wise distributions at $Y/b = 0.6$ (the only equipped section with Kulite sensors) of the clean and controlled configurations are compared in Fig. 9. The rms is computed for a signal length equal to 4s. For the three controlled configurations, the maximum level corresponding to the crossing of the shock is located at about $X/c = 0.55$. More downstream, the pressure fluctuation levels are lower in all controlled configurations than for the baseline. This confirms that unsteadiness in the separated region has been damped with either passive or active control. One can also note that the lowest

levels are obtained by fluidic VGs. However, pressure fluctuation levels at the shock location are greater in the controlled cases than for the baseline even if in the present case, the shock is located between two sensors (see the shock position in Fig. 9) and, consequently, the peak is not visible in the figure.

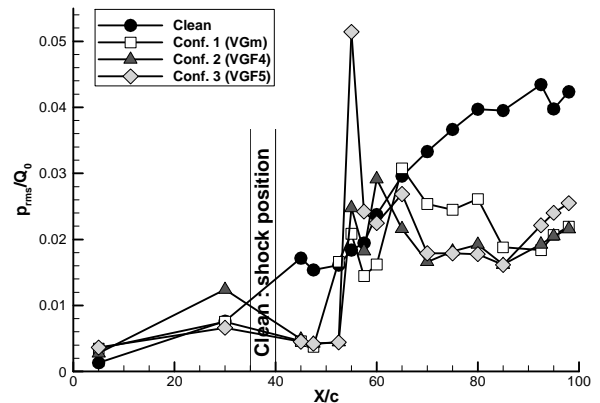


Fig. 9. Comparison of rms pressure distributions between the clean configuration and the controlled ones with mechanical and fluidic VGs ($\alpha = 3.5^\circ$ and $M_0 = 0.82$)

To study the interaction of the vortices created by VGs with the boundary layer and the shock, LDV measurements have been performed in planes parallel to the wing leading edge along the span. Figure 10a shows the iso-values of normalized longitudinal velocity (left) and turbulent kinetic energy (right) in the shock foot region. One notes a decrease of the longitudinal velocity between $Z/c = 0.1$ and 0.065 . This is due to the fact that this measurement plane is located inside the lambda-shock structure including compression waves. Below $Z/c = 0.065$, vortices' wakes are clearly visible, as well as small separations between the vortices at the shock foot. They are characterized by high rms values, and their very spatially limited extensions are visible in oil flow visualizations in Fig. 7 also.

The iso-values of longitudinal velocity and turbulent kinetic energy downstream of the shock are shown in Fig. 10b. The traces of the longitudinal vortices persist despite the crossing through the shock. The turbulent kinetic energy level is decreased behind the shock because the flow is fully reattached.

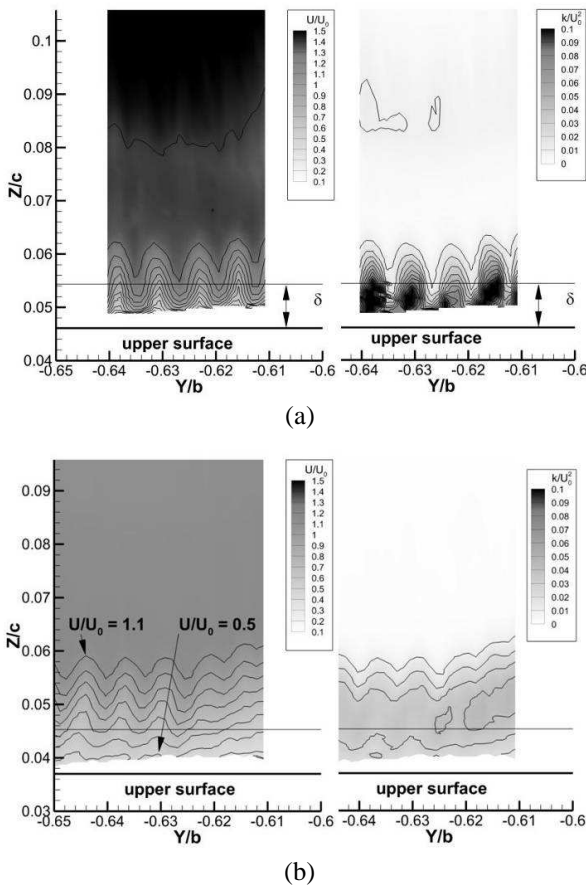


Fig. 10. Iso-values of the longitudinal velocity (left) and the turbulent kinetic energy (right) in the shock foot (a) and downstream of the shock (b), for the controlled configuration with fluidic VGs ($\alpha = 3.5^\circ$ and $M_0 = 0.82$)

5 Towards Laminar Flow Investigations

5.1 Context

Laminar flow at S3Ch wind tunnel has recently become a leading field of research as a result of the efforts towards cleaner aerodynamics. Keeping boundary layers laminar on a large extent of an aircraft surface represents a promising way to reduce the drag and to curb down fuel consumption. However, laminar airfoil aerodynamics remains much less understood than its turbulent counterpart owing to the lower interest it has received up to now. Moreover, the characterization of laminar flows puts at stake both numerical and experimental methods.

Then, these objectives have been undertaken under the research project named “ATLAPT” (Aérodynamique Transsonique et

Laminaire avec Application au Phénomène de Tremblement) financed by the Agence Nationale de la Recherche in France.

5.2 Wind Tunnel Qualification

An essential parameter governing the flow in laminar condition is the quality of the free-stream. The wind tunnel flow quality has thus first been assessed using different techniques. Firstly, an unsteady pressure sensor and a hot wire have been installed in the empty test section of the wind tunnel in order to calculate the N factor of the free stream. Using the formulae given by Mack’s law [8]:

$$N_T = -8.42 - 2.4 \log(Tu)$$

where N_T is value of the N factor at transition and Tu is the free-stream rate of turbulence. Note that we could compare the results obtained by the hot wire to those given by the unsteady pressure probe using the linearized acoustic relation:

$$p' = \rho c u'$$

and calculating a rate of turbulence based on pressure fluctuations. In this relation, c is the speed of sound and ρ is the mean flow density. Turbulence levels of less than 1% were found at transonic speed, giving an N factor approximately equal to 6. This flow quality is in the range of most transonic wind tunnel around the world.

In a second step, a canonical cone was tested and the location of the boundary layer transition was measured by infrared (IR) thermography. Transition is marked in wall temperature fields by a sudden increase of the temperature value. Considering an adiabatic wall assumption, Crocco’s law gives an evaluation of the wall temperature increase during the transition process (the recuperation coefficient is equal to 0.85 and 0.9, respectively in laminar and turbulent regimes, this increase reflecting the higher thermal diffusion imposed by turbulence). For a flow at $M_0 = 0.7$ and $T_{i0} = 320\text{K}$ such as the one produced at S3Ch, this represents a 1.4K increase in temperature. The camera which was used is a FLIR SC7600 with

a resolution of 25mK, which is thus fully able to capture the transition. A hundred images were recorded and averaged prior to post-processing.

The tested model is a cone with a 10° angle introduced at the center of the test section (see Fig. 11). The yaw and roll angles of the cone could be freely adjusted in order to align the cone with the upstream flow. The cone was made of Plexiglas. This material is well suited to IR imagery because it has a low thermal conductivity and a high emissivity (equal to 0.86, close to that of a black body). The typical wall temperature at the cone surface obtained in the course of these tests is shown in Figure 11. Azimuthally average of the temperature field over the range of azimuth seen by the camera was carried out in order to derive the mean position of transition. Comparing the transition location measured experimentally with that predicted by the numerical stability (calculation of the growth of small perturbation in the boundary layer) confirmed the N factor obtained by the previous velocity and pressure fluctuations measurements: the N factor is equal to 5.4 for the free-stream flow of $M_0 = 0.7$.

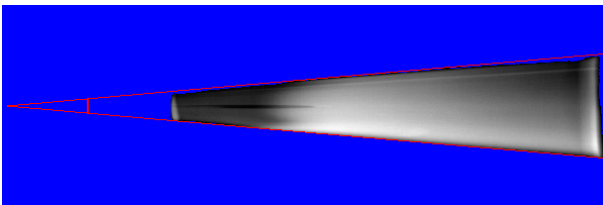


Fig. 11. Wall temperature at the surface of the cone. Grey levels indicate the wall temperature, dark to light indicating warmer temperature. The cone geometry is indicated by the red lines

5.3 Tests on a Supercritical Airfoil

The buffet phenomenon arises in transonic flow condition when the shock wave oscillates. It has been characterized under a turbulent incoming boundary layer at S3Ch wind tunnel in the past [9]. The flow physics obtained in laminar conditions is yet poorly understood. In particular the large excursion of the shock wave observed in turbulent conditions has never been observed when the boundary layer is laminar.

To tackle this problem, tests have been performed with an airfoil relied on the OAT15A supercritical airfoil (see Fig. 12). Model equipment included steady and unsteady wall

pressure sensors and Sacotherm paint for IR imaging. The paint corresponds to the flat grey area visible on the model. Approximately one third of the wingspan is covered. The state of the boundary layer on the upper surface of the wing was monitored by the IR camera installed below the floor of the test section. The view of the upper surface was obtained by looking at its reflection about the roof of the test section through a circular IR glass window installed in the floor. This technique permitted the use of the deformable roof of the test section to accommodate for the compressible effects. To circumvent the diffusion of the transition temperature jump in the highly thermally conductive metallic material of the wing, a palliative measure consisting in varying rapidly the stagnation temperature of the flow was adopted. Doing so artificially increases the contrast between the laminar and turbulent parts of the wing and allows a better determination of the transition location.

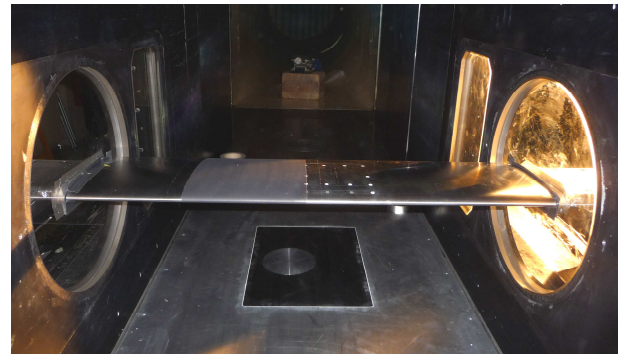


Fig. 12. View of the experimental set-up

As a validation of the experimental set-up, the buffet dynamics in turbulent conditions was first reproduced and compared to previous results [9,10]. The transition of the boundary layer to a turbulent state was obtained by tripping using carborundum grains installed at 7% of chord. Figure 13 shows the pressure spectra obtained upstream of the shock wave when the Mach number is increased from 0.6 to 0.75 at angle of attack $\alpha = 3.5^\circ$. The pressure fluctuations are seen to increase with the Mach number. The appearance of a marked peak around 70Hz at $M_0 = 0.73$ is indicative of the buffet phenomenon. The frequency of the peak slightly shifts when the Mach number is increased further. Strong harmonics dominate

the upper part of the spectra, which denotes the existence of an unstable mode to the flow. The unstable mode could be obtained by numerical simulations of the flow based on a linearized approach recently implemented in the ONERA *elsA* CFD solver [11,12].

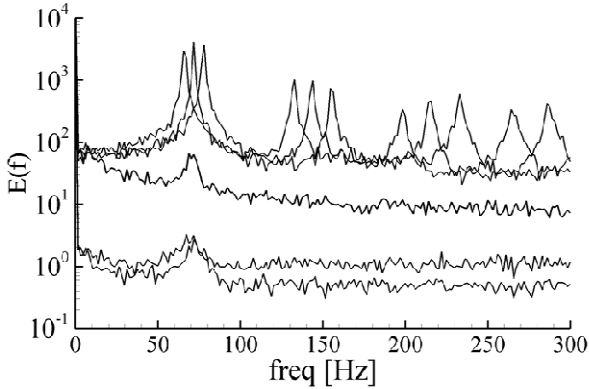


Fig. 13. Pressure spectra obtained in the turbulent condition at the shock foot at increasing Mach number 0.6, 0.68, 0.72, 0.73, 0.74 and 0.75 and $\alpha = 3.5^\circ$

The laminar flow was then tested in the same conditions as the turbulent case without tripping the boundary layer near the airfoil leading edge. The pressure spectrum obtained in the configuration $M_0 = 0.73$ and $\alpha = 3.5^\circ$ is shown in Figure 14. The absence of the buffet peak in the low frequencies is the most spectacular result; instead a pressure peak in the higher frequencies around 1000Hz is seen to appear.

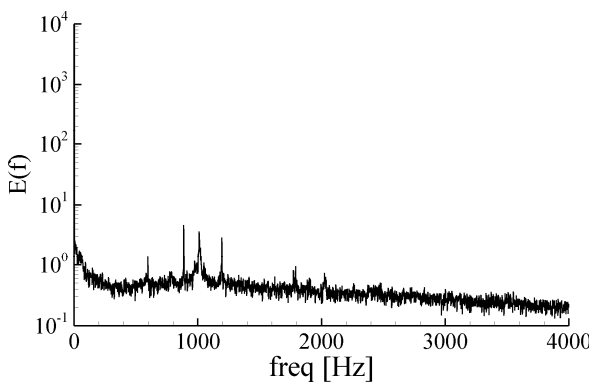


Fig. 14. Pressure spectrum obtained in the laminar condition at $M_0 = 0.73$ and $\alpha = 3.5^\circ$

Work is currently underway to understand this shift in the dynamics of the buffet phenomenon. Possible explanations can be put forward. First the incoming boundary layer being laminar, the shock foot is less disturbed

than in the turbulent case. This sensitivity to external noise may traduce the sub-critical nature of the buffet phenomenon. Moreover, the presence of a (tiny) recirculation bubble at the shock foot, typical of laminar conditions, may also significantly modify the flow topology. The bubble dynamics is the most likely cause of the pressure peak at 1000Hz.

The temperature fields deduced from the IR thermography measurements at the wing upper surface are shown in Figure 15 for the natural transition in the configuration $M_0 = 0.73$ and $\alpha = 3.5^\circ$. The shock wave triggers the transition to the turbulent state in this case.

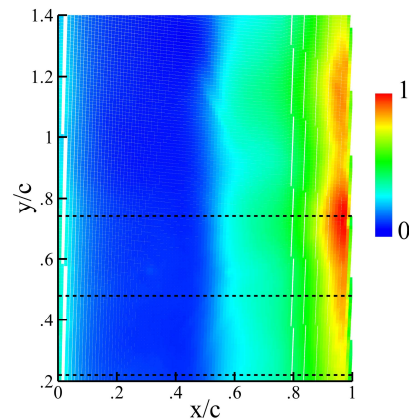


Fig. 15. Temperature distribution mapped to the range [0, 1] on the wing upper surface at $M_0 = 0.73$ and $\alpha = 3.5^\circ$

Post-processing of the temperature images was achieved by extracting three profiles along the dotted lines indicated in Fig. 15, averaging and calculating the chord-wise derivative of the temperature. The location of the transition was taken at the maximum amplitude of the derivative. Figure 16 shows the result obtained on the same case, $M_0 = 0.73$ and $\alpha = 3.5^\circ$.

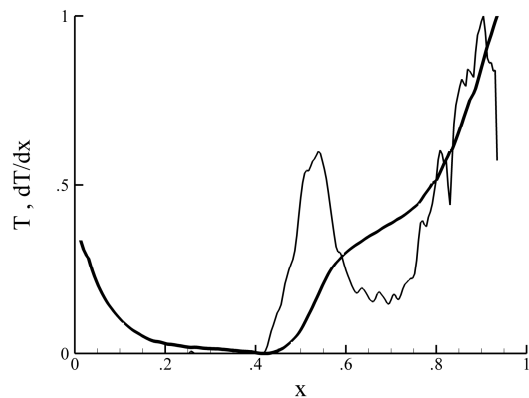


Fig. 16. Profile of temperature and its derivative as a function of chord-wise distance at $M_0 = 0.73$ and $\alpha = 3.5^\circ$

The transition is located at 52% of the chord, almost at the same position as the shock wave.

6 Conclusion

The variety of presented results has demonstrated the capability of the ONERA S3Ch wind tunnel to reproduce complex flow field configurations around various models and to furnish complete database thanks to classical probe-like and optical non-intrusive measurement techniques. These experimental results also served as well-documented test cases for the computational fluid dynamics community to validate advanced computing methods.

Concerning the investigation on the civil aircraft power plant, main results have been used to the design of the shapes of both engine nozzle and pylon with respect to the thermal loads.

The study of control of turbulent buffet over a swept wing is pursuing into the CleanSky Joint Technology Initiative (JTI) project "SFWA - ITD" (Smart Fixed Wing Aircraft - Integrated Technology Demonstrator). The capability of some actuators to control the flow in a closed-loop approach is very challenging.

At last, buffet control on a laminar airfoil will be the main objective defined in the European project "BUTERFLI" (BUffet and Transition delay control investigated within European-Russian cooperation for improved FLIght performance). Both passive (bump) and active (air jet VGs) devices will be tested in the S3Ch wind tunnel.

References

- [1] Pérouze C. *La soufflerie S3 Chalais Meudon - Description de l'installation rénovée en 1987 et de ses moyens d'essais*. ONERA Report RT 117/1865 AN, 2000.
- [2] Brunet V, Molton P, Bézard H and Deck S. Advanced experimental and numerical investigations of an aircraft powerplant configuration. AIAA Paper 2010-4814, *28th AIAA Applied Aerodynamics Conference*, Chicago, Illinois, 28 June - 1 July 2010.
- [3] Jacquin L, Molton P, Deck S, Maury B and Soulevant D. An experimental study of shock

oscillation over a transonic supercritical profile. *AIAA Journal*, Vol. 47, No. 9, pp 1985-1994, 2009.

- [4] Thiery M and Coustols E. Numerical prediction of shock induced oscillations over a 2D airfoil: influence of turbulence modelling and test section walls. *International Journal of Heat and Fluid Flow*, Vol. 27, No. 4, pp 661-670, 2006.
- [5] Coustols E, Brunet V, Bur R, Caruana D and Sipp D. BUFET'N Co: A joint ONERA research project devoted to buffet control on a transonic 3D wing using a closed-loop approach. *CEAS/KATNET II Conference*, Bremen, Germany, 12-14 May 2009.
- [6] Dandois J, Brunet V, Molton P, Abart J-C and Lepage A. Buffet control by means of mechanical and fluidic vortex generators. AIAA Paper 2010-4975, *28th AIAA Applied Aerodynamics Conference*, Chicago, Illinois, 28 June - 1 July 2010.
- [7] Molton P, Dandois J, Lepage A, Brunet V and Bur R. Control of buffet phenomenon on a transonic swept wing. *AIAA Journal*, Vol. 51, No. 4, pp 761-772, 2013.
- [8] Mack L. Transition prediction and linear stability theory. In: *AGARD Conf. Proc. No. 224*, Paris, France, 1977.
- [9] Jacquin L, Molton P, Deck S, Maury B and Soulevant D. Experimental study of shock oscillation over a transonic supercritical profile. *AIAA Journal*, Vol. 47, No. 9, pp 1985-1994, 2009.
- [10] Deck S. Numerical simulation of transonic buffet over a supercritical airfoil. *AIAA Journal*, Vol. 43, No. 7, pp 1556-1566, 2005.
- [11] Sartor F, Mettot C and Sipp D. Global stability analysis of a transonic flow over OAT15A airfoil. *Bulletin of the American Physical Society: 66th Annual Meeting of the APS Division of Fluid Dynamics*, Vol. 58, No. 18, Pittsburgh, Pennsylvania, 24-26 Nov. 2013.
- [12] Sartor F, Mettot C and Sipp D. Stability, receptivity and sensitivity analyzes of buffeting transonic flow over a supercritical profile. Submitted to *AIAA Journal*, 2014.

Contact Author Email Address

mailto:Reynald.Bur@onera.fr

Copyright Statement

The authors confirm that they, and/or their company or organization, hold copyright on all of the original material included in this paper. The authors also confirm that they have obtained permission, from the copyright holder of any third party material included in this paper, to publish it as part of their paper. The authors confirm that they give permission, or have obtained permission from the copyright holder of this paper, for the publication and distribution of this paper as part of the ICAS 2014 proceedings or as individual off-prints from the proceedings.